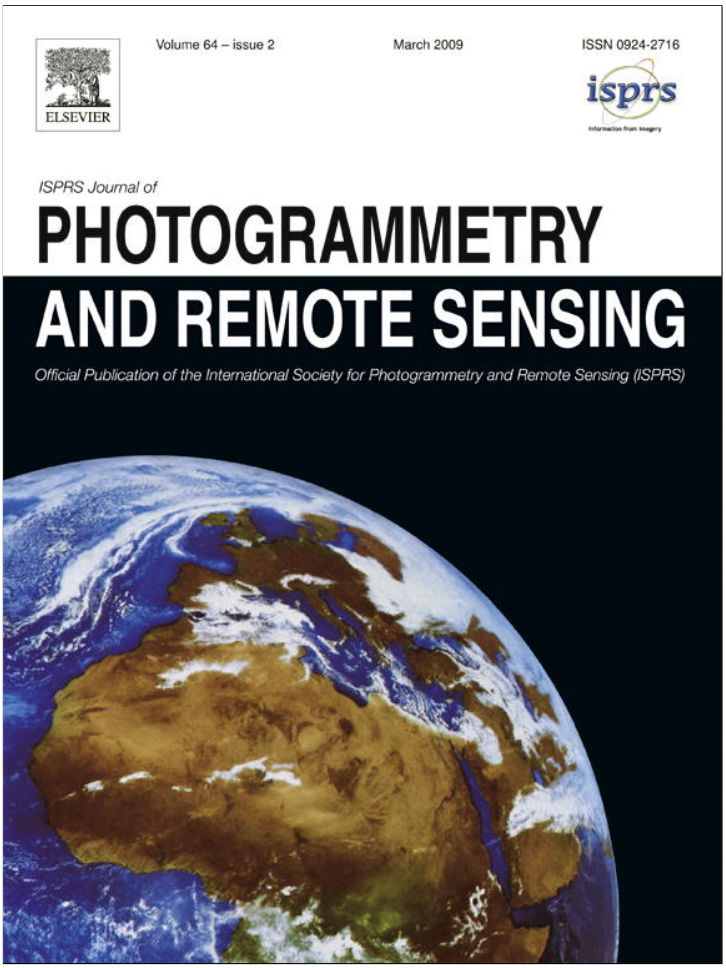

ISPRS Journal of Photogrammetry and Remote Sensing 64 (2009) 151–158

Contents lists available at ScienceDirect

ISPRS Journal of Photogrammetry and Remote Sensing

journal homepage: www.elsevier.com/locate/isprsjprs

Estimating vertical plant area density profile and growth parameters of a wheat canopy at different growth stages using three-dimensional portable lidar imaging

Fumiki Hosoi, Kenji Omasa *

Graduate School of Agricultural and Life Sciences, The University of Tokyo, Yayoi 1-1-1, Bunkyo-ku, Tokyo 113-8657, Japan

ARTICLE INFO

Article history:
Received 4 April 2008
Received in revised form
15 September 2008
Accepted 16 September 2008
Available online 18 October 2008

Keywords:
Carbon stock
Plant area density
Portable scanning lidar
Three-dimensional imaging
Voxel-based canopy profiling

ABSTRACT

Vertical plant area density profiles of wheat (*Triticum aestivum* L.) canopy at different growth stages (tillering, stem elongation, flowering, and ripening stages) were estimated using high-resolution portable scanning lidar based on the voxel-based canopy profiling method. The canopy was scanned three-dimensionally by laser beams emitted from several measuring points surrounding the canopy. At the ripening stage, the central azimuth angle was inclined about 23° to the row direction to avoid obstruction of the beam into the lower canopy by the upper part. Plant area density profiles were estimated, with root mean square errors of 0.28–0.79 m^2 m^{-3} at each growth stage and of 0.45 m^2 m^{-3} across all growth stages. Plant area index was also estimated, with absolute errors of 4.7%–7.7% at each growth stage and of 6.1% across all growth stages. Based on lidar-derived plant area density, the area of each type of organ (stem, leaves, ears) per unit ground area was related to the actual dry weight of each organ type, and regression equations were obtained. The standard errors of the equations were 4.1 g m^{-2} for ears and 26.6 g m^{-2} for stems and leaves. Based on these equations, the estimated total dry weight was from 63.3 to 279.4 g m^{-2} for ears and from 35.8 to 375.3 g m^{-2} for stems and leaves across the growth stages. Based on the estimated dry weight at ripening and the ratio of carbon to dry weight in wheat plants, the carbon stocks were 76.3 g C m^{-2} for grain, 225.0 g C m^{-2} for aboveground residue, and 301.3 g C m^{-2} for all aboveground organs.

1. Introduction

The plant canopy plays important functional roles in cycling materials and energy through photosynthesis and transpiration, maintaining plant microclimates, and providing habitats for various taxa (Ehleringer and Field, 1993; Jones, 1992; Larcher, 2001; Monteith, 1973; Stokes et al., 2006). Determining the vertical structure of the canopy is very important because the three-dimensional (3-D) composition of the canopy helps to sustain those functional roles (Graetz, 1990; Lefsky et al., 2002; Omasa et al., 2007a; Schurr et al., 2006). Thus, many studies have been conducted to measure the vertical structure of plant canopies (Eschenbach and Kappen, 1996; Garber and Maguire, 2005; Hosoi and Omasa, 2006, 2007; Hutchison et al., 1986; Lefsky et al., 2002; Omasa et al., 2007a; Parker et al., 2004; Radtke and Bolstad, 2001; Sinoquet et al., 1998; Strachan and McCaughey, 1996; Wang et al., 1992; Yang et al., 1993).

In crop canopies, the vertical structure has been investigated and related to characteristics such as light distribution within the canopy, light-use efficiency, amount of yield, growth rate, and nitrogen allocation (Constable, 1986; Imai et al., 1994; Milroy et al., 2001; Sassenrath-Cole, 1995; Takahashi and Nakaseko, 1993; Yunusa et al., 1993). As noted in those studies, it is important to account for changes in the vertical structure of crops accompanied with canopy growth over time. The vertical canopy structure is often represented by leaf area density (LAD) in each horizontal layer, which is defined as one-sided leaf area per unit of horizontal layer volume (Weiss et al., 2004). The leaf area index (LAI) is then calculated by vertically integrating the LAD profile data. When it is difficult for leaves and other aboveground organs (e.g., stems, ears) to be separated, then rather than LAD or LAI, plant area density (PAD) or plant area index (PAI) are used.

To obtain LAD and PAD, stratified clipping of leaves has been used as a direct method (Imai et al., 1994; Milroy et al., 2001; Takahashi and Nakaseko, 1993). Although this direct method offers accurate results, its application to crop measurement is often limited because it is very labor intensive and its destructive nature does not permit the measurement of intact crop structure as plants change over time with growth, which is an important parameter in crop studies. 3-D digitizing by ultrasonic or electromagnetic devices has been used as another direct method. A pointer is located at the position of each plant component and geometric

* Corresponding author. Tel.: +81 3 5841 5340; fax: +81 3 5841 8175.
E-mail address: aomasa@mail.ecc.u-tokyo.ac.jp (K. Omasa).

0924-2716/$ – see front matter © 2008 International Society for Photogrammetry and Remote Sensing, Inc. (ISPRS). Published by Elsevier B.V. All rights reserved.
doi:10.1016/j.isprsjprs.2008.09.003

information is recorded as 3-D spatial coordinates (Drouet et al., 1999; Sinoquet et al., 1991, 1998, 2007; Thanisawanyangkura et al., 1997). Although this technique allows measurement of the detailed 3-D structure of plants, including the vertical structure, through nondestructive means, this method is also labor intensive because numerous components must be measured manually, point by point. Therefore, this method is also unfavorable for repeated measurements to capture the temporal changes of crop structure with growth. As an indirect method, the gap-fraction method has been widely applied to crop measurement and uses commercially available tools such as cameras with fish-eye lenses and optical sensors (e.g., the Li-Cor LAI-2000 plant canopy analyzer; Behrens and Diepenbrock, 2006; Bréda, 2003; Grantz et al., 1993; Hanan and Bégué, 1995; Levy and Jarvis, 1999; Sassenrath-Cole, 1995; Welles and Cohen, 1996). This method allows automatic data collection and nondestructive measurement of canopy structure by using light transmittance through the canopy. The shortcoming is that the accuracy of the measurement is affected by the spatial distribution of leaves and by sunlight conditions (Chason et al., 1991; Jonckheere et al., 2004).

Light detection and ranging (Lidar), which is an active remote-sensing technique that uses a laser scanner, has been applied to canopy measurements (Brandtberg et al., 2003; Harding et al., 2001; Holmgren and Persson, 2004; Hosoi et al., 2005; Hosoi and Omasa, 2006, 2007; Hyyppä et al., 2001; Lefsky et al., 2002; Næsset et al., 2004; Omasa et al., 2000, 2002, 2003, 2007a,b; Riaño et al., 2003). Lidar can measure the distance between the sensor and a target based on the elapsed time between the emission and return of laser pulses (the time-of-flight method) or based on trigonometry (the optical-probe or light-section methods), so that 3-D information of the target can be obtained. Several researchers have attempted to measure vertical foliage profiles using portable ground-based nonscanning lidar (Parker et al., 2004; Radtke and Bolstad, 2001). At present, portable ground-based scanning lidar is more often used for the measurement because it allows more efficient data collection than the nonscanning type (Henning and Radtke, 2006; Hosoi and Omasa, 2006, 2007; Lovell et al., 2003; Omasa et al., 2002, 2007a,b; Takeda et al., 2005; Tanaka et al., 2004; Urano and Omasa, 2003; Van der Zande et al., 2006).

Portable ground-based scanning lidar has several beneficial features. For instance, it is nondestructive and, because it is an active sensor, measurements are not affected by the light conditions in the field. Many 3-D data for a crop can be recorded quickly and automatically as 3-D point-cloud data. Finally, portable ground-based scanning lidar is suitable for repeated measurements over time due to its efficient data collection and portability. Thus, this technology promises to overcome the shortcomings of the conventional means of measuring the vertical structure of crops. However, portable scanning lidar has been used mainly for measurement of forest canopies and hardly has been utilized for crop measurement, because many crops have small canopies and most of the commercially available portable lidar systems were insufficient for the detailed measurement of crop canopy in terms of scan and range resolution (typically ~cm). Recently, we demonstrated that the vertical LAD profile of small individual trees and 3-D shapes of individual vegetable crops can be measured accurately using high-resolution portable scanning lidar, which has a range resolution of about 1 mm at a measurement range of about 5 m (Hosoi and Omasa, 2006; Omasa et al., 2007a). These findings suggest that high-resolution portable scanning lidar would provide accurate estimation of the vertical structure of crops.

In this study, the vertical canopy profiles of a crop (wheat, *Triticum aestivum* L.) were estimated at different growth stages using high-resolution portable scanning lidar. PAD was the variable used to express the vertical canopy profile. The estimation results were compared with directly measured values to validate the approach. PAI was also estimated by integrating the PAD estimates vertically and was compared with the directly measured value. Based on our findings, ways to obtain growth parameters related to the lidar-derived PAD, namely the dry weight of each organ type and carbon stocks were proposed.

2. Material and methods

2.1. Plant material

The experiment was conducted at an experimental farm in Ibaraki Prefecture, 40 km northeast of central Metropolitan Tokyo, Japan (36°03'N, 140°04'E). Winter wheat (*T. aestivum* cv. Norin 61) seeds were sown on 2 November 2005 using 90 kg seed grain/ha and 50-cm row spacing. Four plots (1 m × 1 m, see Fig. 1A) were established on the farm for measurements of four different growth stages.

2.2. Direct measurements

To obtain validation data, LAD and PAD values were directly measured in each horizontal layer by stratified clipping within each plot on 6 April, 26 April, 16 May, and 5 June 2006 (155, 175, 195, and 215 days after sowing [DAS], respectively), which corresponded to the tillering, stem elongation, flowering, and ripening stages, respectively. On each measurement date, all the plants within each plot were clipped at each 10-cm thickness horizontal layer and the clippings were separated into each type of aboveground organ (leaf, stem, and ear). Areas of leaf, stem, and ear in each horizontal layer were measured using a commercially available desktop scanner (FB636U, Canon, Inc., Japan); each type of organ in each layer was scanned as a JPEG image (826 × 1165 pixels) and the areas were determined by multiplying the number of pixels of each type of organ in each layer by the area per pixel (Hosoi and Omasa, 2006). PAD of each type of organ in each layer, which is defined as the projected area of each type of organ per unit of horizontal layer volume, was derived by dividing the area of each organ type by the horizontal layer volume (0.1 m^3: 1 m × 1 m in horizontal area × 0.1 m in thickness). PAI was obtained as the vertical integration of PAD of all organs. LAI was also obtained by vertically integrating PAD of leaves (i.e., LAD). In addition, to examine the proportion of PAD of each organ type over time, the PAD values of each organ type were averaged vertically at each growth stage, and the ratio of the mean PAD of each organ type to that of all organs was calculated at each growth stage. After the PAD measurement, all of the organs were dried in an oven at 80 °C for 3 days, and the dry weight of each type of organ in each layer was measured.

2.3. Lidar measurements

A portable high-resolution scanning lidar that calculates distances based on trigonometry (a modified TDS-130L 3-D laser scanner; Pulstec Industrial Co., Ltd., Japan) was used to measure the canopy structure. The measurement was carried out prior to the destructive sampling described above. The lidar's measurable range is 3.5–10 m. The range and scan resolutions are about 1 and 2 mm, respectively, at a measurement range of about 5 m. A rotating mount with a stepper motor and a galvano mirror within the lidar head automated the horizontal and vertical scanning.

Fig. 1A illustrates an aerial view of the wheat canopy measurement by the portable scanning lidar, with several scanning positions surrounding the canopy. Arrows A1–A4 and B1–B4 in Fig. 1A show the directions corresponding to the central azimuth angles of laser beams (φ_c in Fig. 1A) emitted from each of the

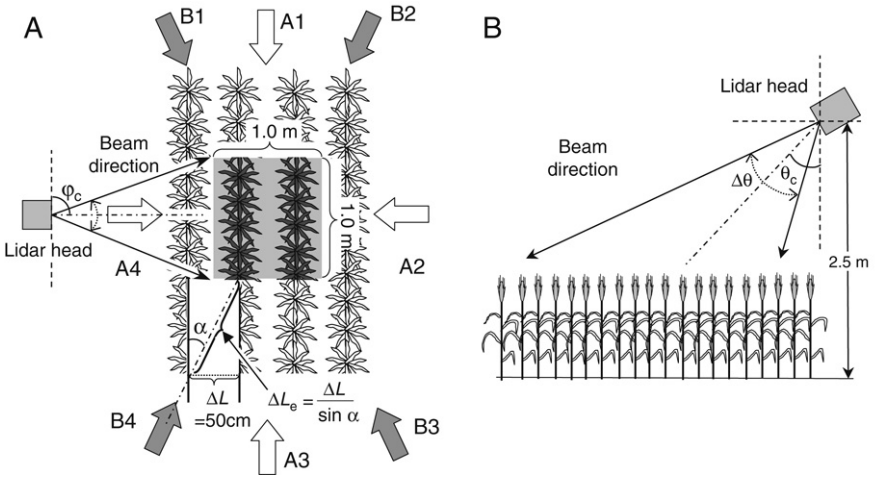

Fig. 1. Schematic view of wheat canopy measurement by high-resolution portable scanning lidar. (A) Aerial view. φ_c represents the central azimuth angle of laser beams. Arrows show the directions corresponding to the central azimuth angles for beams emitted from each measurement position. The rectangle gray region shows the measurement plot. ΔL and ΔL_e represent row spacing and effective row spacing. α represents angle between the directions of the central azimuth angles (B1–B4) and the row direction. (B) Side view. θ_c and $\Delta\theta$ show the central zenith angle and the zenith scan angle of the laser beams.

measurement positions. In this study, the azimuth angle was defined as the angle between azimuth direction of a laser beam and row direction. The central azimuth angle refers to the central angle of the azimuthal laser beam scan. Fig. 1B shows a side view of the wheat canopy measurement. A lidar head was placed at a height of 2.5 m and the central zenith angle (θ_c), which is the center of the angle of the zenith laser beam scan, and its scan angle ($\Delta\theta$) were set to 57.5° and 5°, respectively.

On 6 April, 26 April, and 16 May, directions A1 to A4, which were parallel and perpendicular to the row direction, were applied. On 5 June, directions B1–B4, which inclined about 23° to the row direction (corresponding to $\alpha = 23°$ in Fig. 1A), were applied to increase the number of laser beams that reached the lower layers of the canopy.

2.4. Computation of plant area density

PAD computation used the Voxel-based Canopy Profiling method (VCP method; Hosoi and Omasa, 2006). The complete data set for each date was composed of point-cloud data obtained from each of the four central azimuth angles of laser beams. The individual coordinate systems for these data were registered into a single point-cloud data set with a common 3-D coordinate system for each measurement date using the iterative closest-point algorithm (Besl and McKay, 1992). All points in the registered data set were converted into voxel coordinates for each measurement date. In this experiment, voxel element size, which depended on the range and scan resolution of the lidar, was set to 1 mm. The selection of the voxel element size comparable to the lidar resolution (about 1 and 2 mm) is necessary for the lidar data to be faithfully reproduced as voxels in the voxel array. Voxels converted from points within the registered data set were assigned 1 as the attribute value. Next, all laser beams emitted from the lidar positions were traced within the voxel array in accordance with the actual laser beam angles. Voxels through which one or more laser beams passed without touching the canopy were assigned 2 as the attribute value (see Hosoi and Omasa (2006)).

Based on the attribute values, PAD was computed in each horizontal layer using the following equation:

$$\mathrm{PAD} = \frac{\cos\theta_c}{G(\theta_c)} \cdot \frac{1}{\Delta H} \sum_{k=m_h}^{m_{h+\Delta H}} \frac{n_l(k)}{n_l(k) + n_P(k)}. \quad (1)$$

Eq. (1) is derived from the equation for LAD in Hosoi and Omasa (2006). In Eq. (1), LAD was replaced with PAD and θ_c is the central zenith angle of laser beams,$n_l(k)$ and $n_P(k)$ are the numbers of voxels with attributes of 1 and 2 in the kth horizontal layer of the voxel array, respectively. $n_l(k)$ and $n_P(k)$ represent the number of laser beams intercepted by canopy in the kth layer and the number of laser beams that passed through the kth layer, respectively. Thus, $n_l(k) + n_P(k)$ represents the total number of incident laser beams that reach the kth layer. $\Delta H$is the horizontal layer thickness (=0.1 m), and m_h and $m_{h+\Delta H}$ are the voxel coordinates on the vertical axis equivalent to the height h and $h + \Delta H$ in orthogonal coordinates ($h = m_h \times \Delta k$). $G(\theta_c)$ is the mean projection of a unit leaf area on a plane perpendicular to the direction of the laser beam at θ_c (Jonckheere et al., 2004; Norman and Campbell, 1989; Weiss et al., 2004; Welles and Norman, 1991). Eq. (1) is analogous to the equation of radiation transfer through canopy in the case of neglecting the scattering term (Anisimov and Fukshansky, 1993; Ross, 1981). $n_l(k) + n_P(k)$ and $n_l(k)$ in Eq. (1) correspond to the radiation intensity and the attenuation of the radiation intensity in the radiation transfer equation. The term $\cos(\theta_c)[G(\theta_c)]^{-1}$ is a correction factor for the influence of leaf inclination angle and laser beam direction. Normally, measurement of the distribution of leaf inclination angles is required to determine the correction factor of $\cos(\theta_c)[G(\theta_c)]^{-1}$. However, the central zenith angle of 57.5° used in this study was the particular angle at which $\cos(\theta_c)[G(\theta_c)]^{-1}$ can be considered nearly independent of leaf inclination, so the correction factor was approximated by the constant value of 1.1 (Jonckheere et al., 2004; Warren-Wilson, 1960; Weiss et al., 2004).

From the PAD estimates computed for each horizontal layer, the vertical PAD profile for each measurement date was obtained and compared with the directly measured one. The PAI estimate at each growth stage was obtained by vertical integration of PAD estimates and compared with the directly measured value.

2.5. Estimation of dry weight and carbon stock from lidar-derived plant area density

Ears had developed in the upper layers on 16 May and 5 June. By multiplying the lidar-derived PAD at the upper layers by the ratio of ear to total surface area of each layer on each date obtained from direct measurements, the PAD estimates corresponding to ears were separated. The PAD was converted into area of ears per unit ground area in each horizontal layer by multiplying the PAD values by layer thickness (=0.1 m). The lidar-derived area of ears

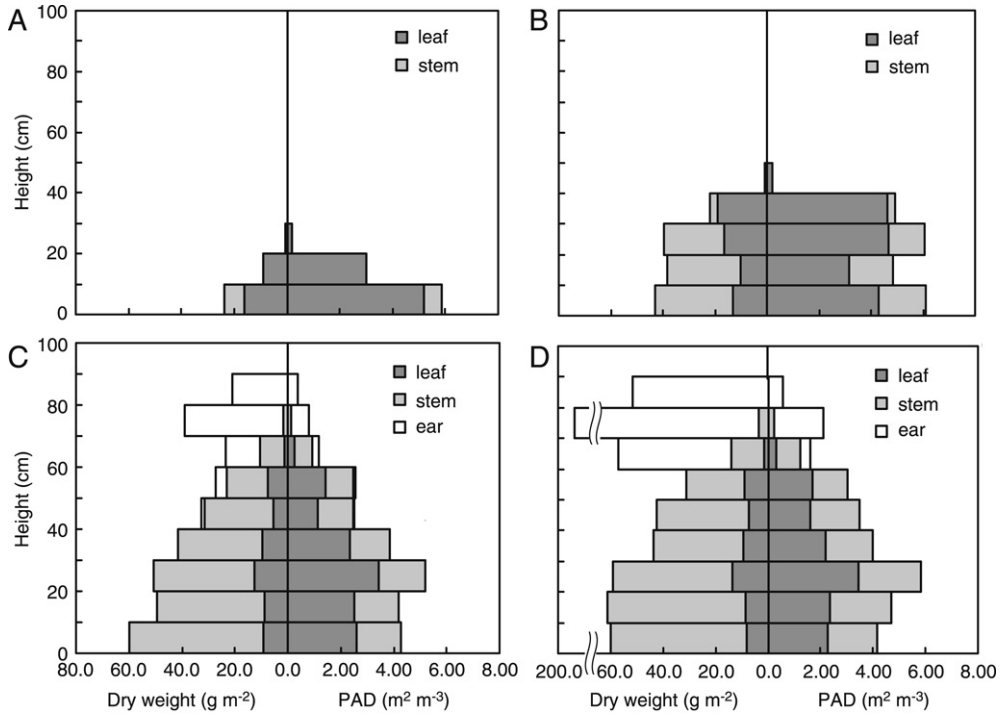

Fig. 2. Directly measured vertical PAD and dry weight distributions of leaf, stem, and ear within a wheat canopy by stratified clipping: (A) 6 April, 155 DAS, tillering stage; (B) 26 April, 175 DAS, stem elongation; (C) 16 May, 195 DAS, flowering; (D) 5 June, 215 DAS, ripening.

was correlated with the corresponding actual ear dry weight, and a regression equation and standard error were obtained. By applying each lidar-derived area of ears to the regression equation, the estimate of ear dry weight in each layer was obtained. Estimates of total dry weight of ears for 16 May (flowering) and 5 June (ripening) were obtained by summing up the estimated dry weight of each layer for each date.

The lidar-derived total area of stems and leaves at each growth stage was obtained by multiplying the lidar-derived PAD by the layer thickness and integrating the values vertically at each growth stage. The total area of stems and leaves on 16 May and 5 June was calculated by subtracting the PAD value of ears from the total for each date. The lidar-derived area of stems and leaves was correlated with the corresponding actual stem and leaf dry weight, and a regression equation and standard error were calculated. By applying each lidar-derived total area of stems and leaves to the regression equation, estimates of the total dry weight of leaves and stems at each growth stage were obtained.

The grain dry weight estimate for 5 June (ripening stage) was separated from the total ear dry weight estimate for that date by using the ratio of grain to ear, 0.7 (Kernan et al., 1984; Sivakumar et al., 2001). The carbon stock within the grain was estimated by multiplying the grain dry weight by the ratio of carbon to dry weight in wheat grain, 0.39 (Huang et al., 2007). Chaff dry weight estimate (i.e., ear dry weight minus grain dry weight) and the total dry weight estimate of leaves and stems on 5 June were summed to obtain the dry weight estimate of aboveground residue. The carbon stock within the aboveground residue on 5 June was estimated by multiplying the dry weight by the ratio of carbon to dry weight in the residue, 0.49 (Huang et al., 2007; IPCC, 2000). By adding the carbon stocks of grain to that of the residue, the total amount of aboveground carbon stock on 5 June was obtained.

3. Results and discussion

The directly measured values of PAD and dry weight of each type of organ are shown in Fig. 2. PAD was distributed at low heights on 6 April (Fig. 2A), but the height distribution expanded upward with stem elongation (Fig. 2B–D). Peaks in the PAD distribution were observed in the lower part of the canopy on 16 May and 5 June and ears shared the upper part of the canopy at those stages (Fig. 2C, D). The proportion of PAD of each organ type changed according to stem and ear development over time (Fig. 3).While leaves accounted for the greatest proportion at the tillering and stem elongation stages (6 and 26 April), the proportion of leaves decreased and that of stems and ears increased at the flowering and ripening stages (16 May and 5 June). The change of the proportion occurred because the development of leaves had already stopped during the latter two stages but stems and ears continued to develop. The values of PAI on 6 April, 26 April, 16 May, and 5 June were 0.90, 2.21, 2.50, and 2.94 m^2 m^{-2}, respectively, and the values of LAI on these dates were 0.83, 1.70, 1.37, and 1.38 m^2 m^{-2}, respectively. The dry weight in each layer changed as the canopy grew (Fig. 2). The contribution of leaves to total dry weight was less than that of other organs, except on 6 April. During the flowering and ripening stages, most of the dry weight

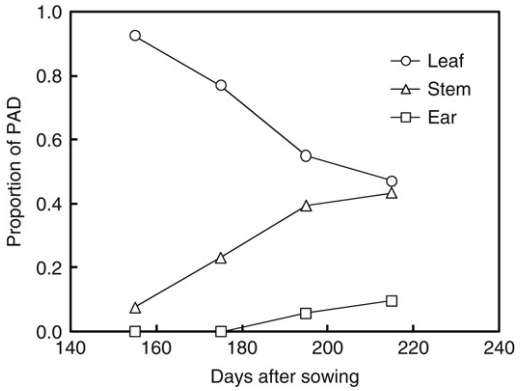

Fig. 3. Change in proportion of directly measured PAD of each organ type over time. The proportions were derived from the vertical mean values of PAD of each organ type at each growth stage.

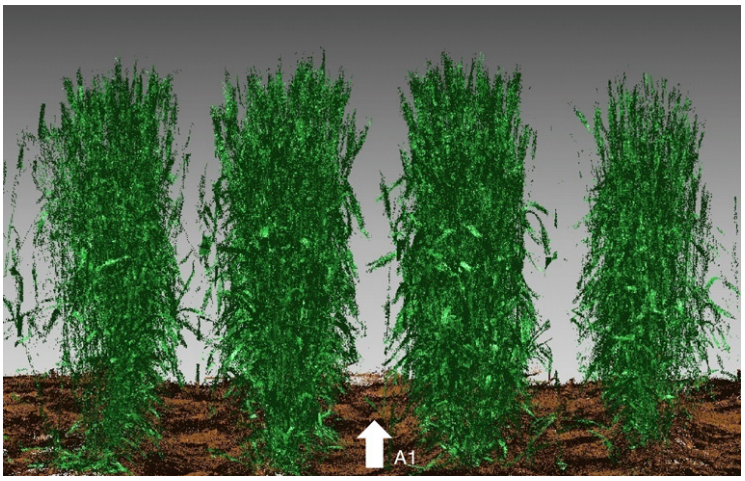

Fig. 4. A 3-D image of wheat canopy on 16 May measured by high-resolution portable scanning lidar. This image was obtained after registration of the images measured by the four central azimuth angles of laser beams (A1–A4 in Fig. 1A). Shading effect was added to this image by changing brightness of each point.

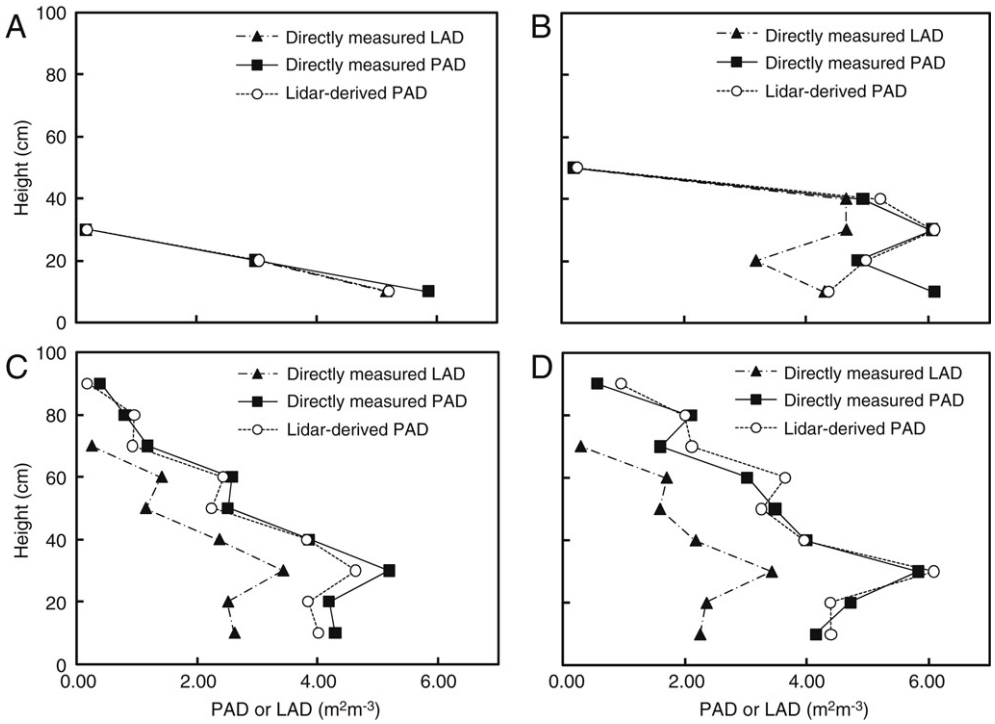

Fig. 5. Comparison of profiles among lidar-derived PAD, directly measured PAD, and directly measured LAD at each growth stage: (A) 6 April, 155 DAS, tillering stage; (B) 26 April, 175 DAS, stem elongation; (C) 16 May, 195 DAS, flowering; (D) 5 June, 215 DAS, ripening.

was composed of ears and stems. The values of total dry weight of all organs on 6 April, 26 April, 16 May, and 5 June were 33.4, 143.8, 345.0, and 606.6 g m^{-2}, respectively. Total ear dry weights for 15 May and 5 June were 76.4 and 292.1 g m^{-2}.

Fig. 4 shows a 3-D lidar image of the wheat canopy on 16 May after registration of the images measured by the four central azimuth angles of laser beams (A1–A4 in Fig. 1A). In the image, shading effect was added by changing brightness of each point. Each leaf shape is distinguishable due to the precise image obtained by high-resolution portable lidar.

Profiles of the lidar-derived PAD estimates and directly measured PAD and LAD are compared in Fig. 5. Changes in the vertical PAD profiles that accompanied the development of plant organs (i.e., leaf development, Fig. 5A, B; stem elongation, Fig. 5B, C; ear development, Fig. 5C, D) was captured well by the accurate PAD estimates, except for underestimation of the lower layers on 6 and 26 April and 16 May. On 5 June, such an underestimation of the lower part was hardly observed, while a slight overestimation was observed in the upper region (>60-cm height). The root-mean-square errors (RMSE) of PAD estimates were 0.38, 0.79, 0.28, and 0.35 m^2 m^{-3} for 6 April, 26 April, 16 May, and 5 June, respectively, and 0.45 m^2 m^{-3} across all the growth stages. Absolute errors of PAI estimates were 6.5%, 5.6%, 7.7%, and 4.7% for these dates, respectively, and 6.1% across all the growth stages. Fig. 6 illustrates the overall relationship between directly measured and lidar-derived PAD across all the growth stages; the lidar-derived values agreed well with the directly measured values ($R^2 = 0.95$).

The following quadratic regression equation shows the relationship between ear dry weight DW_e (g m^{-2}) and lidar-derived area of ears per unit ground area A_e (m^2 m^{-2}):

$$DW_e = 4854.4A_e^2 + 202.3A_e \quad (2)$$

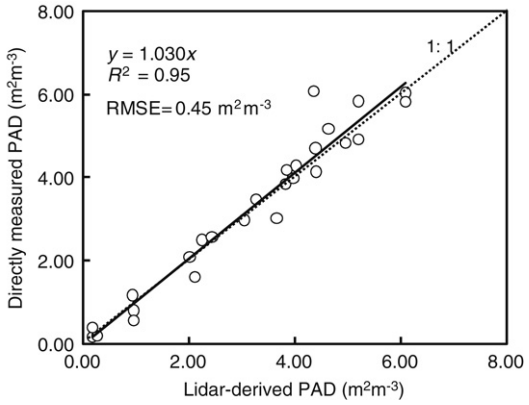

Fig. 6. Relationship between directly measured and lidar-derived PAD through all growth stages. RMSE, root-mean-square error.

($R^2 = 0.96$, SE = 4.1 g m^{-2}; Fig. 7A). Using Eq. (2), the total ear dry weight was estimated as 63.3 and 279.4 g m^{-2} for 16 May and 5 June, respectively. The following regression equation represents the relationship between dry weight of stems and leaves DW_{s+l} (g m^{-2}) and lidar-derived area of stems and leaves per unit ground area A_{s+l} (m^2 m^{-2}):

$$DW_{s+l} = 12.714 \exp(1.228 A_{s+l}). \quad (3)$$

($R^2 = 0.94$, SE = 26.6 g m^{-2}; Fig. 7B). From Eq. (3), the total dry weight of stems and leaves was estimated as 35.8, 164.7, 183.7, and 375.3 g m^{-2} for 6 April, 26 April, 16 May, and 5 June, respectively. Based on these dry weight estimates, the carbon stock of grain on 5 June was estimated to be 76.3 g C m^{-2} and that of aboveground residue was 225.0 g C m^{-2}, such that the total amount of carbon stocks for all aboveground organs on 5 June was estimated to be 301.3 g C m^{-2}.

We previously reported that several measurement points surrounding the canopy and optimally inclined laser beams facilitate full laser beam penetration into the internal canopy, resulting in accurate estimation of the vertical canopy profiles (Hosoi and Omasa, 2006). This was also the case in the present study, as shown by the overall agreement between directly measured and lidar-derived PAD values (Figs. 5 and 6). Having the laser beams inclined at a central zenith angle of 57.5° served well not only for laser beam penetration but also for effective correction of leaf inclination without leaf angle measurements (Hosoi and Omasa, 2006, 2007; Jonckheere et al., 2004; Weiss et al., 2004). At the lowest layers on 6 and 26 April, it appears that there was an insufficient number of laser beams reaching the stems located in the inner canopy; on these dates leaves with the high LAD values in the lower layers would cause obstruction to laser beam penetration into the internal canopy. On 16 May, directly measured LAD values in the lower layers decreased compared with those on 6 and 26 April (Fig. 2C). Although this would facilitate laser beam penetration into the internal canopy of the lower layers, the upper part of the canopy began to obstruct laser beam incidences into the lower layers, in particular for the laser beams directed along A2 and A4 (Fig. 1A).

Fig. 8 illustrates the effects of canopy height and row spacing on laser beam obstruction. At short canopy height, laser beams can reach from the upper to the lower part of the canopy (Fig. 8A). As the canopy grows taller, however, laser beams cannot reach the lower part of the canopy because the upper part obstructs the beam (Fig. 8B). The case in Fig. 8A satisfies the following condition:

$$h \leq \frac{\Delta L}{\tan \theta_c} \quad (4)$$

where h is the canopy height, ΔL is the row spacing, and θ_c is the central zenith angle of the laser beams. In this case, the zenith angles of all incident laser beams are approximated by θ_c. Thus, underestimation of PAD in the lower layers on 16 May (Fig. 5C) would be due to obstruction of the beams by the upper canopy. However, obstruction by the upper canopy can be avoided if the row spacing is expanded such that condition (4) is satisfied (see Fig. 8C). In the present study, instead of expanding row spacing, on 5 June the directions of the central azimuth angles were inclined about 23° with respect to the row direction (B1–B4 in Fig. 1A). In this configuration, effective row spacing ΔL_e (Fig. 1A) is expressed as follows:

$$\Delta L_e = \frac{\Delta L}{\sin \alpha} \quad (5)$$

where α is the angle between the laser beam direction and the row direction. ΔL_e was estimated to be 2.6 times longer than ΔL when $\alpha = 23°$, as in the present experiment. That is, changing the azimuth inclination of the laser beam with respect to the row direction would have the same effect as expanding the row spacing. This change likely led to the improvement of PAD estimates in the lower layers on 5 June. The condition of α necessary to avoid obstruction by the upper canopy (α_c) is given by replacing ΔL in Eq. (4) with ΔL_e in Eq. (5), as follows:

$$\alpha \leq \alpha_c = \arcsin\left[\frac{\Delta L}{h \tan \theta_c}\right]. \quad (6)$$

In the measurement on 5 June, α_c was calculated as 21°. The measurement positions and angular setting of lidar on 5 June were determined based on the criterion that α be as close as possible to α_c.

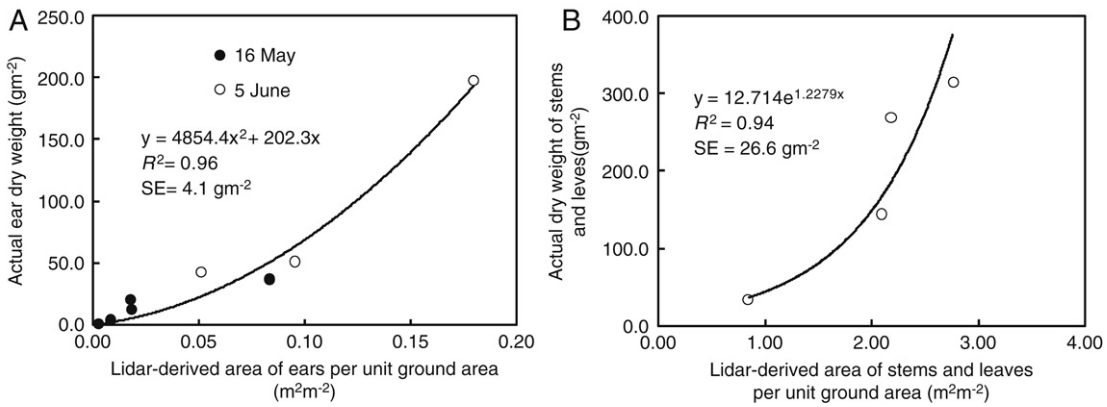

Fig. 7. Relationships between lidar-derived area per unit ground area and actual dry weight. (A) Ears (B) Stems and Leaves. SE, standard error.

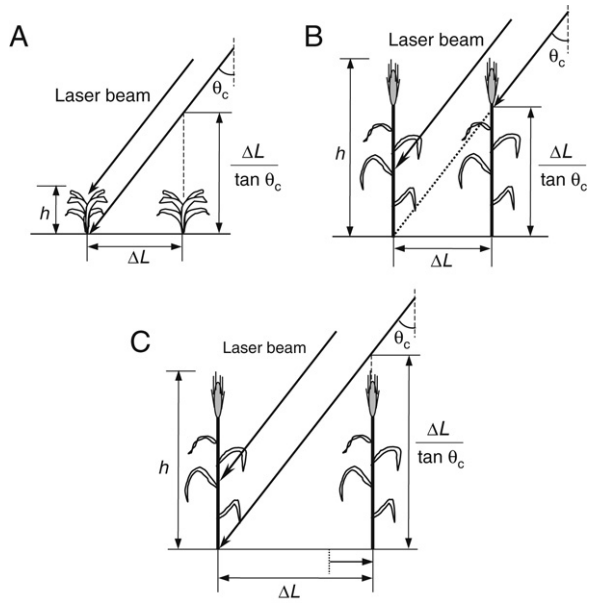

Fig. 8. The effects of canopy height and row spacing on laser beam obstruction. (A) At short canopy height, laser beams can reach from the upper to the lower part of the canopy. ΔL is the row spacing, h is the canopy height, and θ_c is the central zenith angle of laser beams. (B) At tall canopy height, laser beams cannot reach the lower part of the canopy. (C) By expanding row spacing, laser beams can reach the lower part of canopy.

4. Conclusion

The present findings indicate that the dry weight of ears, leaves and stems can be estimated from the regression equation between the dry weight and lidar-derived area of each type of organ. Dry weight estimates can provide useful information about the growing conditions of crops, and lidar-derived data could be used for more effective agricultural management.

Accurate estimation of carbon stocks in plants is important not only to study photosynthetic characteristics but also to estimate global carbon budget affected by recent increase in atmospheric CO_2 concentration that causes global changes. Thus far, lidar has been used mainly for the estimation of forest carbon stocks (Kotchenova et al., 2004; Lim et al., 2003; Omasa et al., 2002, 2003; Patenaude et al., 2004). However, the present study showed that portable scanning lidar also can be used to estimate carbon stocks in a crop canopy. Thus, lidar-derived data sets can be utilized for the estimation of carbon budgets in agricultural regions.

This study demonstrated that vertical PAD profiles of a crop (wheat) canopy at different growth stages can be estimated by high-resolution portable scanning lidar based on the VCP method. In addition, the dry weight and carbon stocks of each organ type can be estimated based on the PAD-derived area of each organ type and the relationship between dry weight and area. To enhance the applicability of portable scanning lidar on estimation of PAD and other growth parameters, additional studies that apply the present method to different growing conditions in other fields and different kinds of crops are needed. Moreover, processing lidar data with additional information, such as shape, color, and texture, may allow lidar data to separate out each organ type so that PAD may be estimated for each organ type. In particular, ears have a distinctive shape and color compared with other organs, so the use of this additional information might allow the efficient separation of ears from other plant organs.

References

Anisimov, O., Fukshansky, L., 1993. Light-vegetation interaction: A new stochastic approach for description and classification. Agricultural and Forest Meteorology 66 (1–2), 93–110.

Behrens, T., Diepenbrock, W., 2006. Using hemispherical radiation measurements to predict weight-related growth traits in oilseed rape (*Brassica napus* L.) and barley (*Hordeum vulgare* L.) canopies. Journal of Agronomy and Crop Science 192 (6), 465–474.

Besl, P.J., McKay, N.D., 1992. A method for registration of 3-D shapes. IEEE Transactions on Pattern Analysis and Machine Intelligence 14 (2), 239–256.

Brandtberg, T., Warner, T.A., Landenberger, R.E., McGraw, J.B., 2003. Detection and analysis of individual leaf-off tree crowns in small footprint, high sampling density lidar data from the eastern deciduous forest in North America. Remote Sensing of Environment 85 (3), 290–303.

Bréda, N.J.J., 2003. Ground-based measurements of leaf area index: A review of methods, instruments and current controversies. Journal of Experimental Botany 54 (392), 2403–2417.

Chason, J.W., Baldocchi, D.D., Huston, M.A., 1991. A comparison of direct and indirect methods for estimating forest canopy leaf area. Agricultural and Forest Meteorology 57 (1–3), 107–128.

Constable, G.A., 1986. Growth and light receipt by mainstem cotton leaves in relation to plant density in the field. Agricultural and Forest Meteorology 37 (4), 279–292.

Drouet, J.L., Moulia, B., Bonhomme, R., 1999. Do changes in the azimuthal distribution of maize leaves over time affect canopy light absorption? Agronomie 19 (3–4), 281–294.

Ehleringer, J.R., Field, C.B., 1993. Scaling physiological processes - leaf to globe. Academic Press, San Diego.

Eschenbach, C., Kappen, L., 1996. Leaf area index determination in an alder forest: A comparison of three methods. Journal of Experimental Botany 47 (302), 1457–1462.

Garber, S.M., Maguire, D.A., 2005. The response of vertical foliage distribution to spacing and species composition in mixed conifer stands in central Oregon. Forest Ecology and Management 211 (3), 341–355.

Graetz, R.D., 1990. Remote sensing of terrestrial ecosystem structure: An ecologist's pragmatic view. In: Hobbs, R.J., Mooney, H.A. (Eds.), Remote Sensing of Biosphere Functioning. Springer, New York, pp. 5–30.

Grantz, D.A., Zhang, X.J., Metheney, P.D., Grimes, D.W., 1993. Indirect measurement of leaf area index in Pima cotton (*Gossypium barbadense* L.) using a commercial gap inversion method. Agricultural and Forest Meteorology 67 (1–2), 1–12.

Hanan, N.P., Bégué, A., 1995. A method to estimate instantaneous and daily intercepted photosynthetically active radiation using a hemispherical sensor. Agricultural and Forest Meteorology 74 (3–4), 155–168.

Harding, D.J., Lefsky, M.A., Parker, G.G., Blair, J.B., 2001. Laser altimeter canopy height profiles methods and validation for closed-canopy, broadleaf forests. Remote Sensing of Environment 76 (3), 283–297.

Henning, J.G., Radtke, P.J., 2006. Ground-based laser imaging for assessing three-dimensional forest canopy structure. Photogrammetric Engineering and Remote Sensing 72 (12), 1349–1358.

Holmgren, J., Persson, Å, 2004. Identifying species of individual trees using airborne laser scanner. Remote Sensing of Environment 90 (4), 415–423.

Hosoi, F., Omasa, K., 2006. Voxel-based 3-D modeling of individual trees for estimating leaf area density using high-resolution portable scanning lidar. IEEE Transactions on Geoscience and Remote Sensing 44 (12), 3610–3618.

Hosoi, F., Omasa, K., 2007. Factors contributing to accuracy in the estimation of the woody canopy leaf-area-density profile using 3D portable lidar imaging. Journal of Experimental Botany 58 (12), 3464–3473.

Hosoi, F., Yoshimi, K., Shimizu, Y., Omasa, K., 2005. 3-D measurement of trees using a portable scanning lidar. Phyton - Annales Rei Botanicae 45 (4), 497–500.

Huang, Y., Zhang, W., Sun, W., Zheng, X., 2007. Net primary production of Chinese croplands from 1950 to 1999. Ecological Applications 17 (3), 692–701.

Hutchison, B.A., Matt, D.R., McMillen, R.T., Gross, L.J., Tajchman, S.J., Norman, J.M., 1986. The architecture of a deciduous forest canopy in eastern Tennessee. USA Journal of Ecology 74 (3), 635–646.

Hyyppä, J., Kelle, O., Lehikoinen, M., Inkinen, M., 2001. A segmentation-based method to retrieve stem volume estimates from 3-D tree height models produced by laser scanners. IEEE Transactions on Geoscience and Remote Sensing 39 (5), 969–975.

Imai, K., Shimabe, K., Tanaka, K., Kawana, T., 1994. Studies on matter production of edible canna (*Canna edulis* Ker.). Japanese Journal of Crop Science 63 (2), 345–351.

IPCC., 2000. Good practice guidance and uncertainty management in national greenhouse gas inventories. IPCC National Greenhouse Gas Inventories Programme. http://www.ipcc-nggip.iges.or.jp/public/gp/english/(Accessed April 4, 2008).

Jonckheere, I., Fleck, S., Nackaerts, K., Muys, B., Coppin, P., Weiss, M., Baret, F., 2004. Review of methods for in situ leaf area index determination. Part I. Theories, sensors and hemispherical photography. Agricultural and Forest Meteorology 121 (1–2), 19–35.

Jones, H.G., 1992. Plants and microclimate, 2nd ed. Cambridge University Press, Cambridge.

Kernan, J.A., Coxworth, E.C., Crowle, W.L., Spurr, D.T., 1984. The nutritional value of crop residue components from several wheat cultivars grown at different fertilizer levels. Animal Feed Science and Technology 11 (4), 301–311.

Kotchenova, S.Y., Song, X., Shabanov, N.V., Potter, C.S., Knyazikhin, Y., Myneni, R.B., 2004. Lidar remote sensing for modeling gross primary production of deciduous forests. Remote Sensing of Environment 92 (2), 158–172.

Larcher, W., 2001. Physiological plant ecology, 4th ed. Springer, Heidelberg.

Lefsky, M.A., Cohen, W.B., Parker, G.G., Harding, D.J., 2002. Lidar remote sensing for ecosystem studies. Bioscience 52 (1), 19–30.

Levy, P.E., Jarvis, P.G., 1999. Direct and indirect measurements of LAI in millet and fallow vegetation in HAPEX-Sahel. Agricultural and Forest Meteorology 97 (3), 199–212.

Lim, K., Treitz, P., Baldwin, K., Morrison, I., Green, J., 2003. Lidar remote sensing of biophysical properties of tolerant northern hardwood forests. Canadian Journal of Remote Sensing 29 (5), 658–678.

Lovell, J.L., Jupp, D.L.B., Culvenor, D.S., Coops, N.C., 2003. Using airborne and ground-based ranging lidar to measure canopy structure in Australian forests. Canadian Journal of Remote Sensing 29 (5), 607–622.

Milroy, S.P., Bange, M.P., Sadras, V.O., 2001. Profiles of leaf nitrogen and light in reproductive canopies of cotton (*Gossypium hirsutum*). Annals of Botany 87 (3), 325–333.

Monteith, J.L., 1973. Principles of environmental physics. Edward Arnold, London.

Næsset, E., Gobakken, T., Holmgren, J., Hyyppä, H., Hyyppä, J., Maltamo, M., Nilsson, M., Olsson, H., Persson, Å, Söderman, U., 2004. Laser scanning of forest resources: The Nordic experience. Scandinavian Journal of Forest Research 19 (6), 482–499.

Norman, J.M., Campbell, G.S., 1989. Canopy structure. In: Pearcy, R.W., Ehleringer, J., Mooney, H.A., Rundel, P.W. (Eds.), Plant Physiological Ecology: Field Methods and Instrumentation. Chapman and Hall, London, pp. 301–325.

Omasa, K., Akiyama, Y., Ishigami, Y., Yoshimi, K., 2000. 3-D remote sensing of woody canopy heights using a scanning helicopter-borne lidar system with high spatial resolution. Journal of Remote Sensing Society of Japan 20 (4), 394–406.

Omasa, K., Hosoi, F., Konishi, A., 2007a. 3D lidar imaging for detecting and understanding plant responses and canopy structure. Journal of Experimental Botany 58 (4), 881–898.

Omasa, K., Hosoi, F., Uenishi, T.M., Shimizu, Y., Akiyama, Y., 2007b. Three-dimensional modelling of an urban park and trees by combined airborne and portable on-ground scanning LIDAR remote sensing. Environmental Modeling and Assessment. doi:10.1007/s10666-007-9115-5.

Omasa, K., Qiu, G.Y., Watanuki, K., Yoshimi, K., Akiyama, Y., 2003. Accurate estimation of forest carbon stocks by 3-D remote sensing of individual trees. Environmental Science & Technology 37 (6), 1198–1201.

Omasa, K., Urano, Y., Oguma, H., Fujinuma, Y., 2002. Mapping of tree position of *Larix leptolepis* woods and estimation of diameter at breast height (DBH) and biomass of the trees using range data measured by a portable scanning lidar. Journal of Remote Sensing Society of Japan 22 (5), 550–557.

Parker, G.G., Harding, D.J, Berger, M.L., 2004. A portable LIDAR system for rapid determination of forest canopy structure. Journal of Applied Ecology 41 (4), 755–767.

Patenaude, G., Hill, R.A., Milne, R., Gaveau, D.L.A., Briggs, BBJ., Dawson, T.P., 2004. Quantifying forest above ground carbon content using LiDAR remote sensing.. Remote Sensing of Environment 93 (3), 368–380.

Radtke, P.J., Bolstad, P.V., 2001. Laser point-quadrat sampling for estimating foliage-height profiles in broad-leaved forests. Canadian Journal of Forest Research 31 (3), 410–418.

Riaño, D., Meier, E., Allgöwer, B., Chuvieco, E., Ustin, S.L., 2003. Modeling airborne laser scanning data for the spatial generation of critical forest parameters in fire behavior modeling. Remote Sensing of Environment 86 (2), 177–186.

Ross, J., 1981. The radiation regime and architecture of plant stands. The Hague, Dr. W. Junk, Netherlands.

Sassenrath-Cole, G.F., 1995. Dependence of canopy light distribution on leaf and canopy structure for two cotton (*Gossypium*) species. Agricultural and Forest Meteorology 77 (1–2), 55–72.

Schurr, U., Walter, A., Rascher, U., 2006. Functional dynamics of plant growth and photosynthesis - from steady-state to dynamics - from homogeneity to heterogeneity. Plant, Cell and Environment 29 (3), 340–352.

Sinoquet, H., Moulia, B., Bonhomme, R., 1991. Estimating the three-dimensional geometry of a maize crop as an input of radiation models: Comparison between three-dimensional digitizing and plant profiles. Agricultural and Forest Meteorology 55 (3–4), 233–249.

Sinoquet, H., Stephan, J., Sonohat, G., Lauri, P.E., Monney, Ph., 2007. Simple equations to estimate light interception by isolated trees from canopy structure features: Assessment with three-dimensional digitized apple trees. New Phytologist 175 (1), 94–106.

Sinoquet, H., Thanisawanyangkura, S., Mabrouk, H., Kasemsap, P., 1998. Characterization of the light environment in canopies using 3D digitising and image processing. Annals of Botany 82 (2), 203–212.

Sivakumar, T., Virendranath, Strivastava, G.C., 2001. Effects of benzyl adenine and abscisic acid on grain yield and yield components in *Triticale* and wheat. Journal of Agronomy and Crop Science 186 (1), 43–46.

Stokes, V.J., Morecroft, M.D., Morison, J.I.L., 2006. Boundary layer conductance for contrasting leaf shapes in a deciduous broadleaved forest canopy. Agricultural and Forest Meteorology 139 (1–2), 40–54.

Strachan, I.B., McCaughey, J.H., 1996. Spatial and vertical leaf area index of a deciduous forest resolved using the LAI-2000 plant canopy analyzer. Forest Science 42 (2), 176–181.

Takahashi, T., Nakaseko, K., 1993. Seasonal changes in distribution of intercepted photosynthetically active radiation for layer and dry matter production in spring wheat canopy. Japanese Journal of Crop Science 62 (2), 313–318.

Takeda, T., Oguma, H., Yone, Y., Yamagata, Y., Fujinuma, Y., 2005. Comparison of leaf area density measured by laser range finder and stratified clipping method. Phyton - Annales Rei Botanicae 45 (4), 505–510.

Tanaka, T., Park, H., Hattori, S., 2004. Measurement of forest canopy structure by a laser plane range-finding method - improvement of radiative resolution and examples of its application. Agricultural and Forest Meteorology 125 (1–2), 129–142.

Thanisawanyangkura, S., Sinoquet, H., Rivet, P., Cretenet, M., Jallas, E., 1997. Leaf orientation and sunlit leaf area distribution in cotton. Agricultural and Forest Meteorology 86 (1–2), 1–15.

Urano, Y., Omasa, K., 2003. Accurate estimation of forest stand parameters in Japanese cedar woods using a portable scanning lidar. In: Proc. IAWPS 2003, Daejeon, Korea, 21–24 April 2003, pp. 403–407.

Van der Zande, D., Hoet, W., Jonckheere, I., van Aardt, J., Coppin, P., 2006. Influence of measurement set-up of ground-based LiDAR for derivation of tree structure. Agricultural and Forest Meteorology 141 (2–4), 147–160.

Wang, Y.S., Miller, D.R., Welles, J.M., Heisler, G.M., 1992. Spatial variability of canopy foliage in an oak forest estimated with fisheye sensors. Forest Science 38 (4), 854–865.

Warren-Wilson, J., 1960. Inclined point quadrats. New Phytologist 59 (1), 1–8.

Weiss, M., Baret, F., Smith, G.J., Jonckheere, I., Coppin, P., 2004. Review of methods for in situ leaf area index (LAI) determination. Part II. Estimation of LAI, errors and sampling. Agricultural and Forest Meteorology 121 (1–2), 37–53.

Welles, J.M., Cohen, S., 1996. Canopy structure measurement by gap fraction analysis using commercial instrumentation. Journal of Experimental Botany 47 (302), 1335–1342.

Welles, J.M., Norman, J.M., 1991. Instrument for indirect measurement of canopy architecture. Agronomy Journal 83 (5), 818–825.

Yang, X., Miller, D.R., Montgomery, M.E., 1993. Vertical distributions of canopy foliage and biologically active radiation in a defoliated/refoliated hardwood forest. Agricultural and Forest Meteorology 67 (1–2), 129–146.

Yunusa, I.A.M., Siddique, K.H.M., Belford, R.K., Karimi, M.M., 1993. Effect of canopy structure on efficiency of radiation interception and use in spring wheat cultivars during the pre-anthesis period in a Mediterranean-type environment. Field Crops Research 35 (2), 113–122.